VII International Conference on Computational Methods in Marine Engineering
MARINE 2017
M. Visonneau, P. Queutey and D. Le Touzé (Eds)

NUMERICAL ASSESSMENT OF INTERFERENCE RESISTANCE FOR A SERIES 60 CATAMARAN

ANDREA FARKAS*, NASTIA DEGIULI* AND IVANA MARTIĆ*

* Faculty of Mechanical Engineering and Naval Architecture (FMENA)
University of Zagreb
Ivana Lučića 5, 10000 Zagreb, Croatia
e-mail: andrea.farkas@fsb.hr, nastia.degiuli@fsb.hr, ivana.martic@fsb.hr, webpage: www.fsb.hr

Key words: Computational Fluid Dynamics (CFD), Volume of Fluid (VOF), *k-ε* turbulence model, interference resistance

Abstract. An important consideration in the catamaran design is the distance between the hulls. Arrangement of the hulls in catamaran configuration can have strong influence on the wave making resistance and thus on the total resistance of a catamaran. The hydrodynamic interaction between hulls becomes significant when spacing between hulls is sufficiently small. In this paper, numerical simulations of viscous flow around monohull and catamaran model are performed utilizing commercial software package STAR-CCM+, in order to investigate the influence of spacing between hulls on the interference resistance. A mathematical model based on Reynolds Avaraged Navier-Stokes (RANS) equations, *k-ε* turbulence model and Volume of Fluid (VOF) method for describing the motion of two-phase media are briefly described. Numerical simulations are performed for Series 60 monohull and two catamaran configurations with C_B=0.6 for different values of Froude number. Results of performed numerical simulations are compared with experimental results available in the literature and satisfactory agreement has been achieved. It has been shown that CFD is a very useful tool in preliminary catamaran design.

1 INTRODUCTION

Catamaran configurations, as well as the other multihull configurations, have attracted attention because of their exquisite performance regarding the speed, safety, resistance, maneuverability and transversal stability. Multihulls have better technical characteristics than monohulls [1] and therefore a significant increase in demand for them can be noticed in the civil, recreational and military field. Even though numerous theoretical, numerical and experimental investigation concerning multihull vessels have been made recently [2], catamaran resistance is still very unpredictable [3]. Due to hydrodynamic interaction between hulls, spacing between them is one of the most important parameters in catamaran design and it must be taken into account at the design stage [4]. The wave systems of each hull usually strongly interfere, causing either favourable or unfavourable effects [5]. As a result of the interference resistance, catamaran resistance is not just a double resistance of the monohull [6]. Because of the significance of the spacing between hulls in catamaran configurations, many authors have investigated the relation between spacing between hulls and the

interference resistance.

Broglia et al. [7] carried out towing tank tests for Delft 372 catamaran and concluded that the interference effects are dominant for small spacing between hulls and at intermediate values of Froude number (*Fn*). At lower *Fn* wave elevations are too small to produce significant effect on the total resistance of a catamaran and at higher *Fn* the individual wave systems of each hull are very diverging and thus superposition between them is considerably reduced. Therefore, a catamaran starts to behave as a combination of almost non-interacting vessels. Trim and sinkage are found to be strongly related with the interference effects.

Due to advancements of computer science and numerical computation methods, the efficiency and accuracy of Computational Fluid Dynamics (CFD) methods are greatly improved. Consequently, the combination of model tests and CFD methods is becoming an optimum choice to analyze hydrodynamic characteristics of a catamaran [8]. Although catamarans have significant growth in popularity, numerical methods for the determination of their hydrodynamic characteristics are rather scarce and incomplete [4]. Haase et al. [9] developed a novel full-scale resistance prediction method for large medium-speed catamarans based on CFD. Their method is based on the assumption that accuracy of pressure drag is independent of Reynolds number (*Rn*). This method can successfully estimate full-scale resistance based on the simulations at full-scale *Rn* without altering the linear dimensions, flow velocity or spatial resolution of the initial model mesh. Broglia et al. [10] have performed numerical simulations for both catamaran and monohull models in order to investigate interference effects and their dependence on *Rn*. These simulations have been performed for fixed models at the dynamic positions taken from the measurements. The analysis of the results showed that interference effects have weak dependence on *Rn*. In [11] Zaghi et al. have presented the results of extensive experimental and numerical studies, performed in order to investigate the interference effects and their dependence on the spacing between hulls. The interference resistance as well as the maximum of the total resistance coefficient are found to be higher for the narrower configurations. Maximum total resistance coefficient occurs at higher *Fn* for the narrower configurations. Interference is considerably affected by the section shape of the demihull [12]. Yengejeh et al. [13] have performed various numerical simulations utilizing solver based on Reynolds Averaged Navier-Stokes (RANS) equations for asymmetric planing hulls at different trim angles, spacing between hulls and *Fn*. Authors have shown that catamaran configuration has significantly reduced wetted surface area than the corresponding monohull having the same displacement.

In this paper, numerical simulations of the viscous flow around monohull and catamaran models are performed utilizing commercial software package STAR-CCM+, in order to study the influence of spacing between hulls on the interference resistance. Mathematical and physical model used in numerical simulations are presented. Thereafter, numerical setup and implemented boundary conditions are given. Numerical simulations are performed for Series 60 monohull and catamaran with C_B=0.6 for *Fn* values in the range from 0.3 to 0.5 and for two spacing between hulls 0.565 m and 0.971 m. Interference resistance is investigated through the interference factor (*IF*). Obtained *IF* are compared with experimental results available in the literature and satisfactory agreement has been achieved.

2 GOVERNING EQUATIONS

Navier-Stokes equations and the continuity equation form a system of coupled, non-linear partial differential equations. Since, they are not solvable for flows around ship hulls, these equations are averaged. Time averaging of Navier-Stokes equations yields to RANS. RANS and averaged continuity equations are given as follows [14]:

$$\frac{\partial\left(\rho\overline{u}_i\right)}{\partial t}+\frac{\partial}{\partial x_j}\left(\rho\overline{u}_i\overline{u}_j+\rho\overline{u_i'u_j'}\right)=-\frac{\partial\overline{p}}{\partial x_i}+\frac{\partial\overline{\tau}_{ij}}{\partial x_j} \tag{1}$$

$$\frac{\partial\left(\rho\overline{u}_i\right)}{\partial x_i}=0 \tag{2}$$

where ρ is the fluid density, $\overline{u}_i$ is the averaged Cartesian components of the velocity vector, $\rho\overline{u_i'u_j'}$ is the Reynolds tensor stress and $\overline{p}$ is the mean pressure. $\overline{\tau}_{ij}$ is the mean viscous stress tensor defined with following equation:

$$\overline{\tau}_{ij}=\mu\left(\frac{\partial\overline{u}_i}{\partial x_j}+\frac{\partial\overline{u}_j}{\partial x_i}\right) \tag{3}$$

where μ is the dynamic viscosity.

For tracking and locating the free surface, Volume of Fluid (VOF) method is used. This method represents volume fraction occupied by some fluid inside an arbitrary closed volume. The volume fraction of water (α_l) is determined according to continuity equation and for incompressible flow reads:

$$\frac{\partial}{\partial t}\alpha_l+\nabla\cdot\left(\alpha_l\overline{u}_i\right)=0 \tag{4}$$

Physical properties of particular fluid depend on the presence of that fluid in the particular cell. If there are only two fluids present in the domain, fluid 1 and fluid 2, density is being calculated according to equation:

$$\rho=\rho_2(1-\alpha_1)+\rho_1\alpha_1 \tag{5}$$

where ρ_1 is the density of the fluid 1, ρ_2 is the density of the fluid 2 and α_1 is the volume fraction of the fluid 1. Other physical properties are calculated analogously according to equation (5).

Most commercial RANS solvers are based on Finite Volume Method (FVM). For description of turbulence effects on averaged flow, *k*-*ε* turbulence model is used together with wall functions. This is two equation model that solves transport equations for turbulent kinetic energy *k* and its dissipation rate *ε*. In this paper, Realizable *k*-*ε* Two-Layer (RKE2L) turbulence model was used. This model generally gives at least as good, or even better results than Standard *k*-*ε* (SKE) turbulence model [15] which was proposed by Lauder and Spalding [16]. RKE2L contains a new transport equation for *ε* and critical coefficient of the model C_μ is no longer constant as in the SKE, but it is instead expressed as a function of a mean flow and turbulence properties. Furthermore, RKE2L can work with low-*Rn* type meshes and with wall

function type meshes. This allows that $y+$ parameter in the first cell can be either smaller than 1 or in the range $30 < y+ < 1000$ [15].

3 COMPUTATIONAL MODEL

In this Section, description of computational model used within this research is presented. Firstly, the model used in numerical simulations is presented, then creation of the virtual towing tank is described and afterwards numerical setup is given.

3.1 Model geometry

Numerical simulations were performed for slightly modified S60 model compared to the one defined as benchmark for Tokyo 1994 CFD Workshop. This model is the same one as used in [5]. Modification is made because the hull geometry of benchmark model for Tokyo 1994 CFD Workshop had too many surface patches with not enough quality matching. Also, in order to cope with waves generated at higher Fn, vertical extension of the hull is made [5]. Body plan of the original S60 geometry [17] and the one used in [5] is shown in Figure 1. It can be seen that matching of these two geometries is satisfactory. The main particulars of the monohull model used in this paper are presented in Table 1. Two different catamaran configurations have been investigated. The alteration is based on the different spacing between hulls s, one catamaran configuration has s=0.565 m (C1) and another one has s=0.971 m (C2).

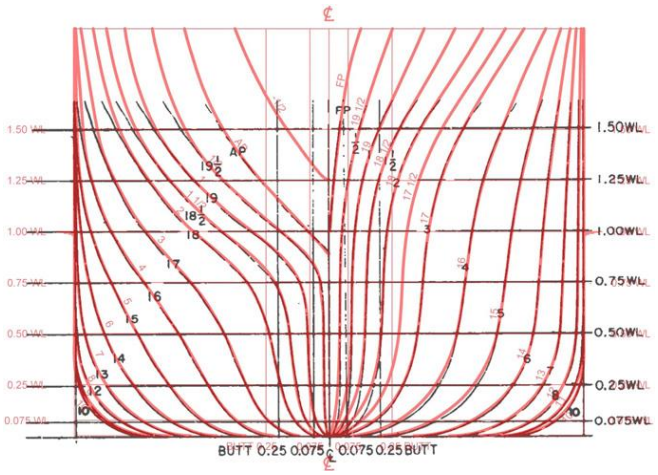

Figure 1: The original S60 bodyplan [17] (black) and the modified bodyplane [5] (red)

Table 1: The main particulars of the monohull model

Main particulars	
Length between perpendiculars (L_{pp})	2.5 m
Beam (B)	0.333 m
Draft (T)	0.133 m
Wetted surface (S)	1.062 m^2
Displacement (Δ)	65.7 kg
Block coefficient (C_B)	0.6

3.2 Virtual towing tank

Virtual towing tank is made by creating a domain around the model hull. All domain boundaries are placed $2L_{pp}$ away from the model. Due to symmetry of the ship model, only half of computational domain is modeled. Thus, for monohull only half of the ship model is considered. For catamaran configuration, only demihull was considered. The centerline of demihull is placed at half of s from the symmetry plane. Unstructured hexahedral mesh is made utilizing meshing tools within STAR-CCM+ as follows: Surface Remesher, Trimmer, Prism Layer Mesher and Automatic Surface Repair. All mesh parameters are defined as relative values of the cell base size, except in the case of Prism Layer Mesher, where prism layer thickness is set as an absolute value in order to keep the same value of $y+$ parameter in the first cell next to the wall. This value is held above 30 in order to ensure that the near-wall cell lies within the logarithmic region of the boundary layer. Prism layer is made with six cells. Two grids with different number of cells are made, coarse (G1) and fine (G2). Coarse grids for both monohull and catamaran configurations had around half of million cells, while fine grid for monohull had around 1.9 million cells and for catamaran configurations around 2.1 million cells. The structure of G2 for monohull and C2 can be seen in Figure 2. Calculated $y+$ at the first cell next to the wall, for monohull with G2 and Fn=0.45 is shown in Figure 3.

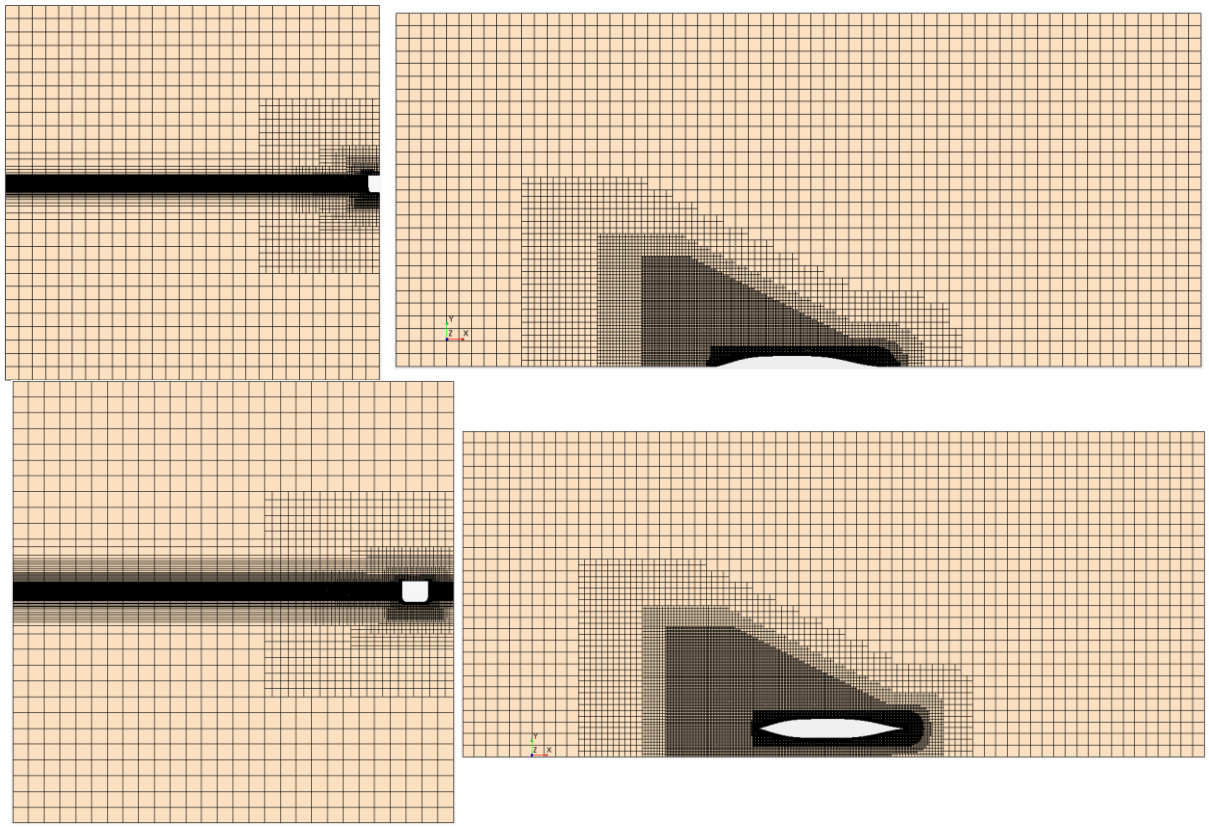

Figure 2: Fine grid G2 for monohull (upper) and for C2 (lower)

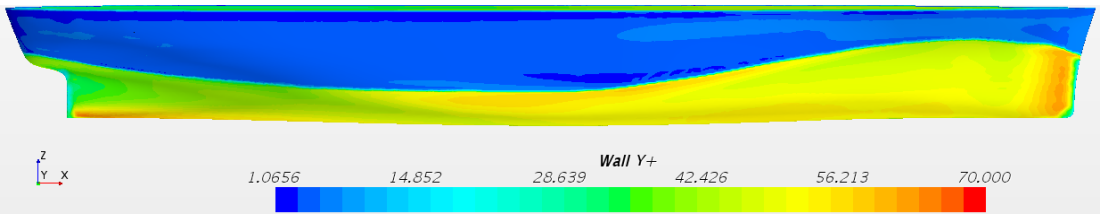

Figure 3: Calculated $y+$ distribution for monohull in the first cell next to the wall for Fn=0.45 with fine grid G2

3.3 Numerical setup

The governing equations described in the Section 2 are discretized using a cell based FVM. Temporal discretization is made using a first-order temporal scheme, also referred as Euler implicit. Convection terms in RANS were discretized with a second-order upwind scheme. Under relaxation factor for velocity is set to 0.7 and for pressure to 0.4. As said before, VOF method is used for modeling the free surface and High Resolution Interface Capturing Scheme (HRIC) is used to track sharp interfaces. Applied boundary conditions are shown in Figure 4.

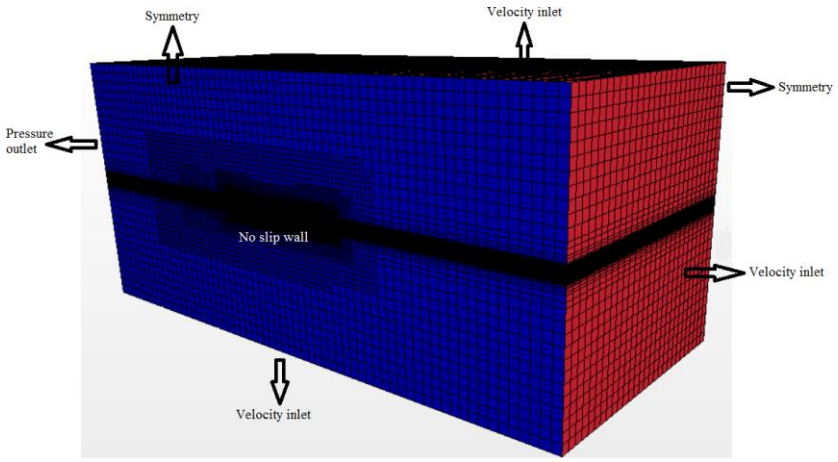

Figure 4: Applied boundary conditions

Time step in every simulation is set to $T/200$, where T is the ratio between L_{pp} and velocity imposed at inlet boundary. Reflection of VOF waves is prevented by importing VOF wave damping at inlet, outlet and side boundary. Implemented approach in STAR-CCM+ is proposed by Choi and Yoon [15]. In this paper, VOF wave damping length is defined using *dvar* function. This function is presented with the following equation:

$$dvar \approx L + L\cos^2\left(\frac{\pi}{2}\frac{t}{10T}\right) \tag{6}$$

This function dampens almost entire area around the ship model at the beginning. As physical time passes, smaller part of the domain is being damped up till $10T$. From then on, half of the domain is damped until the end of simulation. Using the larger damping zone in the beginning of the simulation ensures faster convergence of the results.

4 RESULTS AND DISCUSSION

The total resistance of S60 monohull and two catamaran configurations C1 and C2 is calculated for four different values of *Fn* in the range from 0.3 to 0.5 and the obtained results are compared with experimental results published in [5]. Simulations were performed for fixed models and comparison of the obtained results using two different grid densities with experimental data is shown in Table 2. The obtained results are given as total resistance values, as well as relative deviations (*RD*) from experimental results. *RD* is calculated according to the following equation:

$$RD = \frac{R_T^{\mathrm{CFD}} - R_T^{\mathrm{EXP}}}{R_T^{\mathrm{EXP}}} \tag{8}$$

where R_T^{CFD} is the total resistance obtained utilizing CFD and R_T^{EXP} is the total resistance obtained experimentally.

Table 2: Comparison between experimentally and numerically obtained values of the total resistance

Fn	R_{Tmh}^{E} N	R_{TC1}^{E} N	R_{TC2}^{E} N	R_{Tmh}^{G1} N *RD* (%)	R_{TC1}^{G1} N *RD* (%)	R_{TC2}^{G1} N *RD* (%)	R_{Tmh}^{G2} N *RD* (%)	R_{TC1}^{G2} N *RD* (%)	R_{TC2}^{G2} N *RD* (%)
0.3	5.744	14.429	12.061	6.376 (+11.00)	15.074 (+4.47)	12.880 (+6.79)	6.360 (+10.73)	14.961 (+3.69)	12.721 (+5.47)
0.35	8.643	18.899	17.217	9.217 (+6.64)	19.084 (+0.98)	17.400 (+1.06)	9.167 (+6.06)	19.296 (2.10)	17.675 (+2.66)
0.4	17.089	35.223	43.320	17.991 (+5.28)	35.990 (+2.18)	45.599 (+5.26)	17.967 (+5.14)	36.601 (+3.91)	45.213 (+4.37)
0.5	36.375	98.814	81.635	37.863 (+4.09)	102.411 (+3.64)	85.374 (+4.58)	37.870 (+4.01)	102.243 (+3.47)	85.113 (+4.26)

The results obtained with numerical simulations show satisfactory agreement with experimental results. As it can be seen from Table 2, numerical results overestimate experimental results for monohull and both catamaran configurations for all four values of *Fn*. The overestimation is more significant for monohull for lower values of *Fn*. The greatest relative deviation for monohull using the grid G2 is 10.73% for *Fn*=0.3. It should be mentioned that R_T^{EXP} values are experimentally obtained in kilograms (kg). This means that R_T^{EXP} value for *Fn*=0.3 amounts 0.5855 kg. For such a small value, even small mistake or uncertainty in experimental measurement can lead to relatively high overestimation. The greatest relative deviation for C1 using fine grid G2 is 3.91% and for C2 is 5.47%. The greatest relative deviation obtained using coarse grid G1 for monohull, C1 and C2 are 11.00%, 4.47% and 6.79% respectively.

Within this research, interference resistance of S60 catamaran is investigated through *IF*. *IF* is defined as the ratio of the difference between the total resistance of the catamaran R_{Tcat} and twice the total resistance of the monohull R_{Tmh}, and twice the total resistance of the monohull:

$$IF = \frac{R_{Tcat} - 2R_{Tmh}}{2R_{Tmh}} \tag{7}$$

It should be noted that *IF* can also be calculated considering the wave resistance, but then the total resistance must be decomposed using some decomposition method. In order to obtain the wave resistance, form factor should be known for both catamaran configurations and the monohull. In [5] the form factor is assumed to be identical for both catamaran configurations and the monohull. To avoid error caused by this assumption, *IF* in this paper is calculated on the basis of the total resistance.

IF is calculated for experimentally and numerically obtained results using fine grid G2. Summarized results are given in Table 3 for both catamaran configurations. The curve of *IF* as a function of *Fn* is shown in Figure 5. Even though there are discrepancies between experimentally and numerically obtained *IF*, both curves show the same trend. As it can be seen from Table 3 and Figure 5, values of *IF* are higher for the narrower catamaran configuration except for *Fn*=0.4. This is in accordance with results obtained in [7] and [11]. The minimum of *IF* curve shifts towards higher values of *Fn* for narrower catamaran configuration C1. Value of *Fn* where this minimum occurs is important because at this particular value interference resistance is smallest, even negative for C2.

Table 3: Comparison of experimentally and numerically obtained *IF*

	C1		C2	
Fn	IF^{EXP}	IF^{G2}	IF^{EXP}	IF^{G2}
0.3	0.2560	0.1762	0.0499	0.0001
0.35	0.0933	0.0525	-0.0040	-0.0359
0.4	0.0306	0.0186	0.2675	0.2582
0.5	0.3583	0.3499	0.1221	0.1238

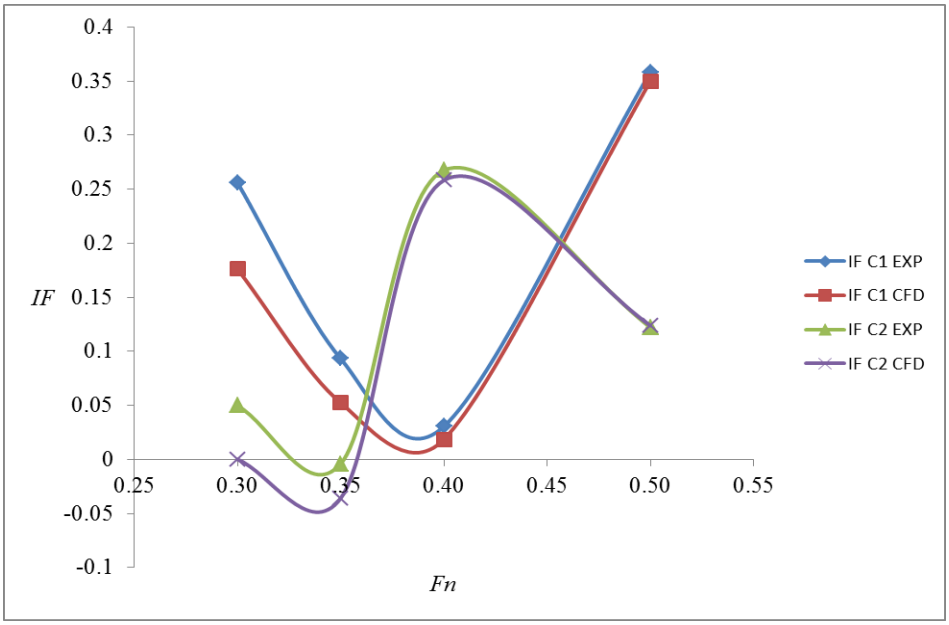

Figure 5: The curve of *IF* as a function of *Fn*

Figure 6. illustrates the wave profile along the monohull and C1 for *Fn*=0.5. This figure shows only starboard side of these two models. The significant change in the wave profile along the catamaran demihull as a result of the interference between the demihulls can be noticed.

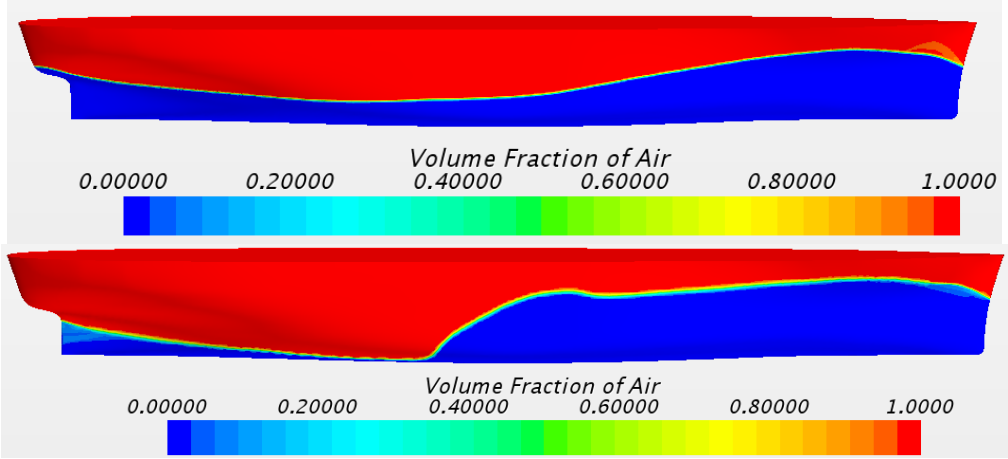

Figure 6: Wave profile along the monohull (upper) and C1 (lower) for *Fn*=0.5

Wave patterns of S60 monohull obtained with fine grid G2 for *Fn*=0.3 and *Fn*=0.5 are shown in Figure 7. It can be noticed that wave elevations are more than two times higher for *Fn*=0.5.

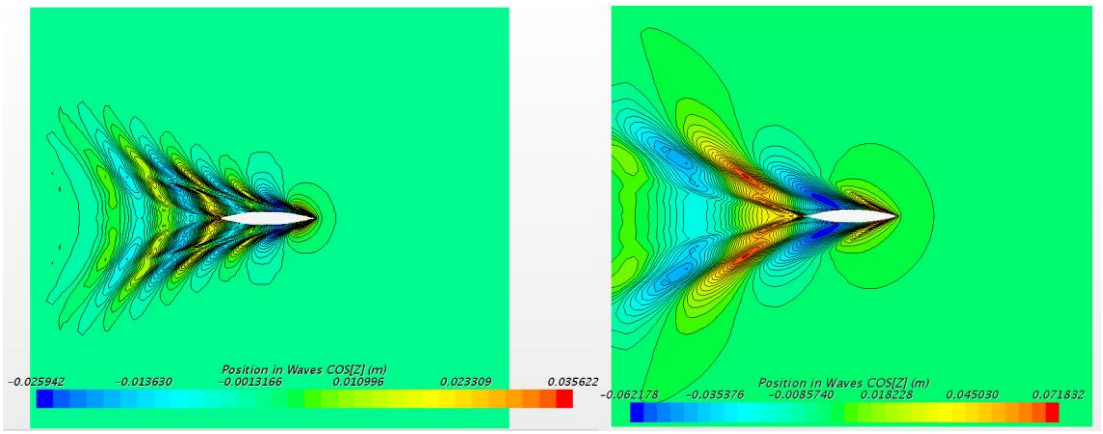

Figure 7: Wave patterns of S60 monohull for *Fn*=0.3 (left) and *Fn*=0.5 (right)

The obtained hydrodynamic pressure distribution on the starboard side and portside of C1 configuration for *Fn*=0.4 can be seen in Figure 8. As it was expected, pressure differences are significantly larger on the starboard side. Wave patterns for both catamaran configurations obtained using fine grid G2 for two *Fn* values are shown in Figure 9. It can be noticed that wave elevations for narrower catamaran configuration are significantly higher than the ones for wider catamaran configuration. The first wave crest behind the monohull and two catamaran configurations is closer to the stern for smaller values of *Fn*. Also, as it can be seen

from Figure 9, the first wave crest is closer to the stern in the case of narrower catamaran configuration.

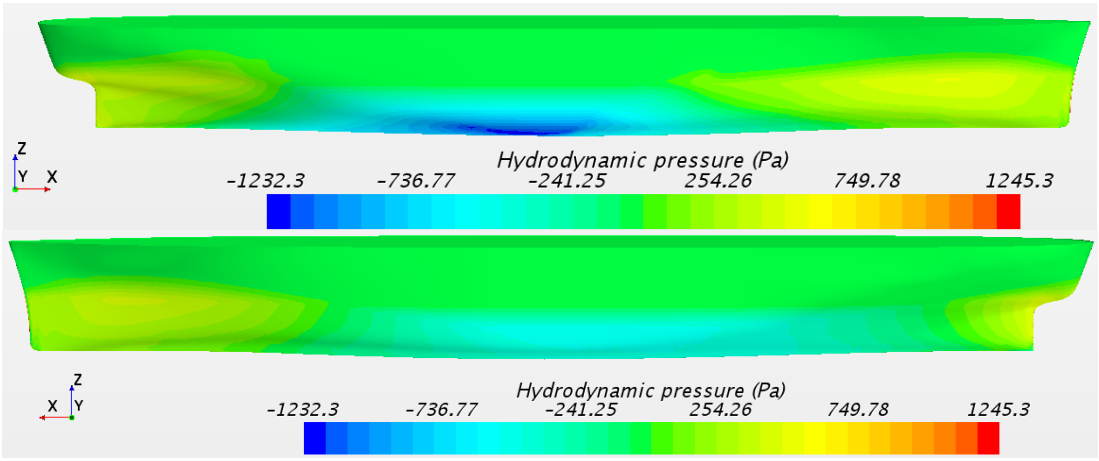

Figure 8: Hydrodynamic pressure distribution on the starboard side (upper) and the portside (lower)

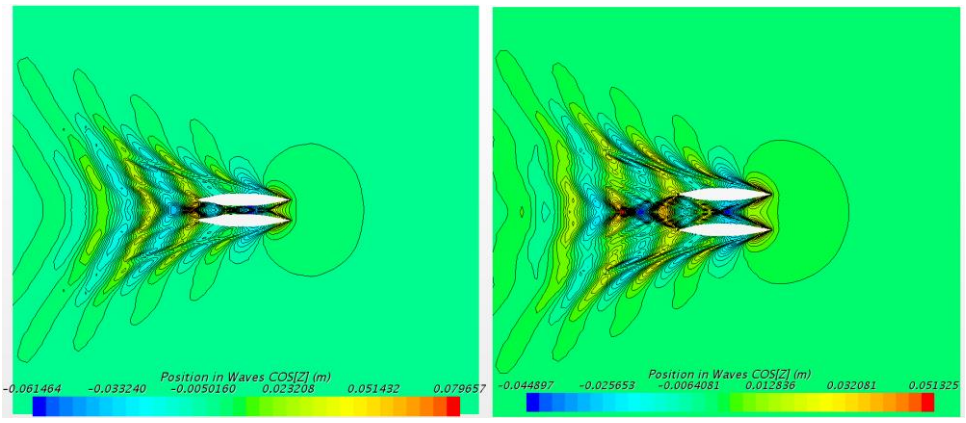

a) Wave pattern of C1 for *Fn*=0.3 b) Wave pattern of C2 for *Fn*=0.3

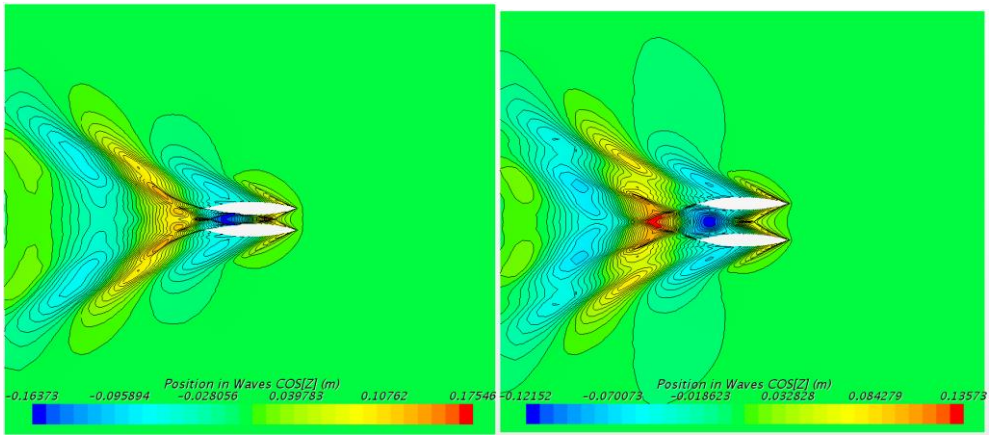

c) Wave pattern of C1 for *Fn*=0.5 b) Wave pattern of C2 for *Fn*=0.5

Figure 9: Wave patterns of C1 (left) and C2 (right) for two *Fn* values

5 CONCLUSION

In this paper, numerical simulations of the viscous flow around the S60 monohull and two catamaran configurations are performed in order to investigate the interference resistance and its dependence on the spacing between hulls. Interference resistance is examined through *IF*. The total resistance obtained with numerical simulations show satisfactory agreement with experimental results, although all values are overestimated. The greatest relative deviations are obtained for lower *Fn* values for the monohull. The uncertainty of measuring resistance for such a small model can be relatively large at lower values of *Fn*. Despite overestimations, the same trend of experimentally and numerically obtained *IF* curves can be noticed. Therefore, it can be concluded that CFD is a very useful tool in catamaran preliminary design. The results point out that interference effects are more significant for narrower catamaran configuration and that the minimum of *IF* curve shifts towards higher values of *Fn*. Also, obtained wave elevations are significantly higher for narrower configuration. The computation data represent a good basis for future studies involving the influence of trim and the arrangement of hulls in catamaran configuration on the interference resistance. Inclusion of some additional goals in finding optimal spacing between hulls, for example seakeeping characteristics, will be investigated in future work.

REFERENCES

[1] Dubrovsky, V. A. Multi-hulls: new options and scientific developments. *Ships and Offshore Structures* (2010) 5(1): 81-92.

[2] Zaghi, S., Broglia, R., Di Mascio, A. Experimental and numerical investigations on fast catamarans interference effects. *Journal of Hydrodynamics* (2010) 22(5): 545-549.

[3] Sahoo, P. K., Salas, M., Schwetz, A. Practical evaluation of resistance of high-speed catamaran hull forms-Part I. *Ships and offshore structures* (2007) 2(4): 307-324.

[4] Bari, G. S., Matveev. K. I. Hydrodynamic modeling of planing catamarans with symmetric hulls. *Ocean Engineering* (2016) 115: 60-66.

[5] Souto-Iglesias, A., Fernández-Gutiérrez, D., Pérez-Rojas, L. Experimental assessment of interference resistance for a Series 60 catamaran in free and fixed trim-sinkage conditions. *Ocean Engineering* (2012) 53: 38-47.

[6] Jamaluddin, A., Utama, I.K.A.P., Widodo, B., Molland, A.F. Experimental and numerical study of the resistance component interactions of catamarans. *Proceedings of the Institution of Mechanical Engineers, Part M: Journal of Engineering for the Maritime Environment* (2012) 227(1): 51-60.

[7] Broglia, R., Jacob, B., Zaghi, S., Stern, F., Olivieri, A. Experimental investigation of interference effects for high-speed catamarans. *Ocean Engineering* (2014) 76: 75-85.

[8] Zha, R., Ye, H., Shen, Z., Wan, D. Numerical computations of resistance of high speed catamaran in calm water. *Journal of Hydrodynamics Ser. B* (2015) 26(6): 930-938.

[9] Haase, M., Zurcher, K., Davidson, G., Binns, J.R., Thomas, G., Bose, N. Novel CFD-based full-scale resistance prediction for large medium-speed catamarans. *Ocean Engineering* (2016) 111: 198-208.

[10] Broglia, R., Zaghi, S., Di Mascio, A. Numerical simulation of interference effects for a high-speed catamaran. *Journal of marine science and technology* (2011) 16(3): 254-269.

[11] Zaghi, S., Broglia, R., Di Mascio, A. Analysis of the interference effects for high-

speed catamarans by model tests and numerical simulations. *Ocean Engineering* (2011) 38(17): 2110-2122.

[12] Sarles, C., Gelles, B., Malarkey, A. An investigation into the effect of section shape on the interference resistance of catamarans. *Proceedings of the 11th International Conference on Fast sea transportation* Hawai.USA. (2011): 355-362.

[13] Yengejeh, M. A., Amiri, M.M., Mehdigholi, H., Seif, M.S., Yaakob, O. Numerical study on interference effects and wetted area pattern of asymmetric planing catamarans. *Proceedings of the Institution of Mechanical Engineers, Part M: Journal of Engineering for the Maritime Environment* (2016) 230(2): 417-433.

[14] Ferziger, J.H. and Perić, M. *Computational Methods for Fluid Dynamics*. Springer Science & Business Media, Berlin, (2012).

[15] STAR-CCM+. User Guide. CD-adapco. (2016).

[16] Launder, B.E. and Spalding, D.B. The numerical computation of turbulent flows. *Computer methods in applied mechanics and engineering* (1974) 3(2): 269-289.

[17] Todd, F.H. Series 60 Methodical Experiments with Models of Single-screw Merchant Ships. Technical report. David W. Taylor Model Basin. (1964).